ACS Photonics

Letter

pubs.acs.org/journal/apchd5

A Comprehensive Photonic Approach for Solar Cell Cooling

Wei Li,[†] Yu Shi,[†] Kaifeng Chen,[†,‡] Linxiao Zhu,[‡] and Shanhui Fan*[,†]

[†]Department of Electrical Engineering, Ginzton Laboratory, and [‡]Department of Applied Physics, Stanford University, Stanford, California 94305, United States

Supporting Information

ABSTRACT: The heating of a solar cell has significant adverse consequences on both its efficiency and its reliability. Here to fully exploit the cooling potential of solar cells, we experimentally characterized the thermal radiation and solar absorption properties of current silicon solar cells and, on the basis of such experimental characterization, propose a comprehensive photonic approach by simultaneously performing radiative cooling while also selectively utilizing sunlight. In particular, we design a photonic cooler made of one-dimensional photonic films that can strongly radiate heat through its thermal emission while also significantly reflecting the solar spectrum in the sub-band-gap and ultraviolet regimes. We show that applying this photonic cooler to a solar panel can lower the cell temperature by over 5.7 °C. We also show that this photonic cooler can be used in a concentrated photovoltaic system to significantly reduce the solar cell temperature or required cooling power. This photonic cooler can be readily implemented in current photovoltaic modules as a retrofit to improve both efficiency and lifetime. Our approach points to an optimal photonic approach for thermal management of solar cells.

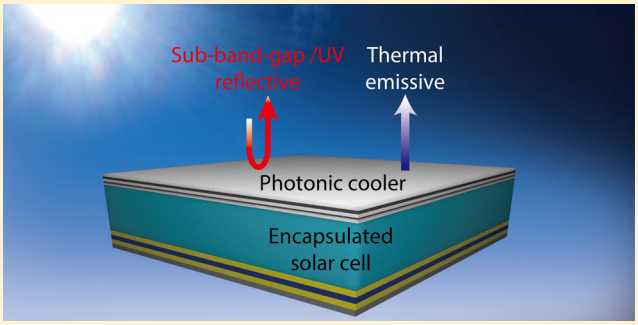

KEYWORDS: *photonics, solar cells, radiative cooling, thermal radiation, radiative heat transfer*

A single-junction solar cell is typically designed to efficiently absorb most incident solar irradiance with photon energy above its semiconductor band gap. However, under the AM1.5 solar spectrum, there is an intrinsic theoretical power conversion efficiency limit of 33.7% based on Shockley and Queisser's analysis,[1] and nowadays most commonly used silicon solar cells possess efficiencies around 15−22%. Therefore, a significant portion of solar energy is converted into heat and, in turn, heats the solar cell. In practice, in outdoor conditions, the typical operating temperature of a solar cell is around 50−55 °C or higher.[2−4] This heating of the solar cell has adverse consequences on both its performance and reliability.[5] The conversion efficiency of the solar cell deteriorates at elevated temperatures. For crystalline silicon solar cells, every 1 °C temperature rise leads to a relative efficiency decline of about 0.45%.[6] In addition, the aging rate of a solar cell array doubles for every 10 °C solar cell temperature increase.[7] Therefore, it is extremely important to develop solar cell cooling techniques to keep the cell operating temperature as low as possible.

Conventional solar cell cooling strategies, including conduction of heat to dissipation surfaces,[8] forced air flow,[9] water cooling,[10] and heat-pipe-based systems,[11,12] have been mainly focused on engineering the nonradiative heat transfer accesses of solar cells using heat conduction or convection approaches. Some of these conductive or convective cooling techniques either need extra energy input or increase the system complexity. On the other hand, radiative heat exchange plays a significant role in the thermal balance of the solar cell. A solar cell is heated by the sun, and moreover it naturally faces the sky and therefore can radiate some of its heat out as infrared radiation. Therefore, complementary to nonradiative approaches, it is also of importance to explore the possibilities of using the photonic approach to engineer the radiative heat transfer access of solar cells for thermal management.

There currently exist two major photonic approaches in the thermal management of solar cells, focusing on controlling either the solar absorption[13−15] or the thermal radiation.[16,17] A solar cell cannot convert sub-band-gap photons to electricity. However, a practical solar cell structure in fact typically has substantial absorption in the sub-band-gap wavelength range. Such sub-band-gap absorption does not contribute to the generation of photocurrent and represents a parasitic heat source. To address this issue, infrared filter design has been proposed to selectively reflect the solar spectrum in the sub-band-gap regime[13−15] to minimize the parasitic heat source. More recently, there is also an emerging interest to design the thermal radiation property of the solar cell for cooling purposes.[16−20] This radiative cooling approach is based on the fact that any sky-facing structure naturally has radiative access to the cold universe through Earth's atmosphere's transparency window between 8 and 13 μm.[16−32] Moreover, since solar cells under sunlight are typically operating above the ambient air temperature, thermal emissions outside the atmosphere transparency window in the entire wavelength range between 4 and 30 μm also help in radiative cooling. Thus,

Received: January 28, 2017
Published: March 14, 2017

DOI: 10.1021/acsphotonics.7b00089
ACS Photonics 2017, 4, 774−782

refs 16 and 17 designed and demonstrated a photonic structure that is transparent in the solar wavelength range, yet behaves as a blackbody in the thermal wavelength range. Such a photonic structure, when placed on a solar cell, can radiatively cool the solar cell underneath it without affecting the solar absorption.

As evidenced from the description above, there are significant opportunities in developing photonic approaches for solar cell cooling. However, the existing approaches, which focus solely on either engineering solar absorption or thermal radiation, can exploit only part of the opportunities that photonic engineering can provide for solar cell cooling purposes. In this paper, we propose a comprehensive photonic strategy for passive cooling of solar cells that can be implemented as a retrofit to current photovoltaic modules (Figure 1). The idea is to place a photonic coating layer on top of the existing encapsulated solar panels. The coating is designed to simultaneously reflect part of the solar spectrum that does not contribute to photocurrent and to maximize thermal radiation. In addition, such a coating serves as a broadband antireflection coating, preserving or even enhancing the optical absorption characteristics of the solar cells in the part of the solar spectrum that contributes to photocurrent. To illustrate the efficacy of this approach, we first provide experimental characterizations of the absorption properties of solar panels in both the solar and thermal wavelength ranges. Based on the experimental data, we then numerically show that a photonic coating structure made of a planar multilayer dielectric stack placed on top of the such solar panels can provide a temperature reduction for the solar cell of over 5.7 K as compared to the same panel without the coating, taking into account the nonradiative heat dissipation processes in a typical terrestrial operating condition.

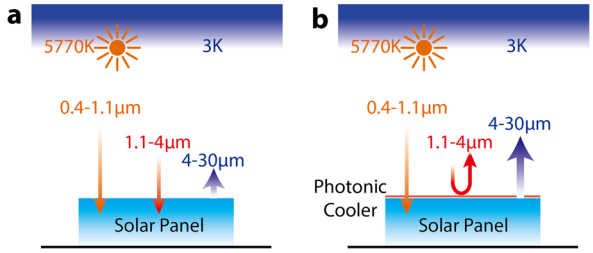

Figure 1. (a) Schematic of the solar absorption and thermal radiation properties of existing solar panels. Suboptimal radiative cooling and strong parasitic sub-band-gap absorption are observed in existing solar panels. (b) With a photonic cooler coated on top of solar panel, the radiative cooling can be enhanced and the sub-band-gap solar radiation can be strongly reflected.

EXPERIMENTAL CHARACTERIZATION OF THE ABSORPTIVITY SPECTRA OF SOLAR CELLS IN THE SOLAR AND THERMAL WAVELENGTH RANGE

To illustrate our photonic approach for solar cell cooling, we first experimentally examine solar absorption (Figure 2a) and thermal emission (Figure 2b) properties of typical commercial solar cells. As examples, we consider crystalline silicon solar cells, which represent solar cells with the highest market penetration.[33] We obtained two types of state-of-the-art bare silicon solar cells: cell I is a silicon solar cell with interdigitated back contacts,[34] and cell II is a silicon solar cell with screen-printed silver front and aluminum rear contacts[35] (Figure 2c). Since in practice in a photovoltaic module a solar cell is always encapsulated, we also encapsulated cell I by sandwiching it with two 0.46 mm thick ethylene-vinyl acetate (EVA) joint interlayers, with a 3.2 mm thick glass as front cover and a 0.5 mm thick back sheet layer made of Tedlar (polyvinyl fluoride), as shown in Figure 2d. The materials and parameters for the

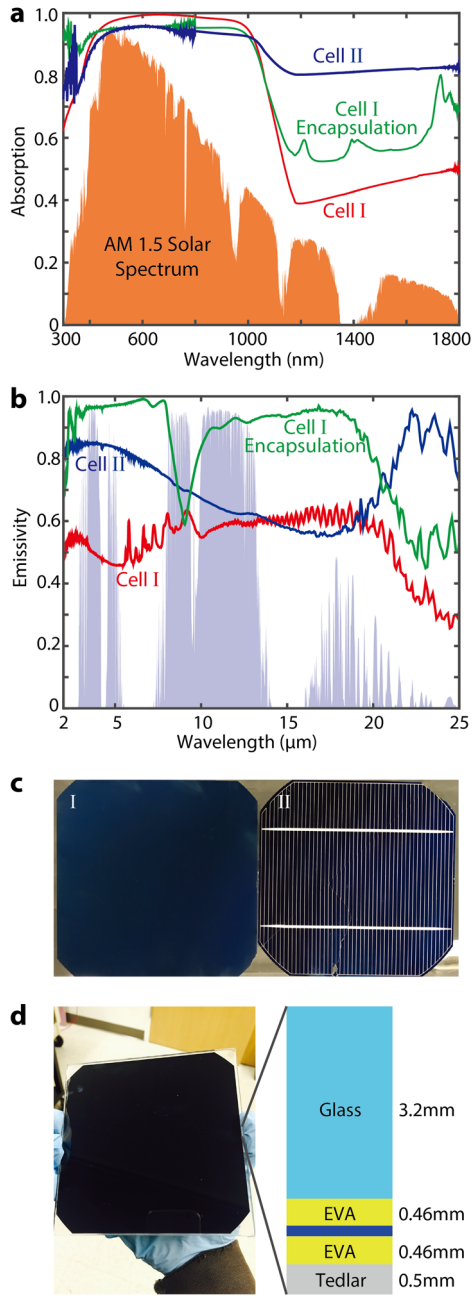

Figure 2. (a) Experimentally measured solar absorption spectra of two representative solar cells and an encapsulated cell, with the normalized AM1.5 solar spectrum plotted for reference. (b) Experimentally measured emissivity spectra of two representative solar cells and an encapsulated cell over the infrared wavelength, with a realistic atmosphere transmittance model from ref 37 for winter in California plotted as the shaded area. (c) Photo of the front side of the two measured solar cells. I: a silicon solar cell with interdigitated back contacts. II: a screen-printed silicon solar cell with silver front and aluminum rear contacts. (d) Photo (left) and a cross-section schematic (right) of a solar cell with encapsulation, made of cell I, with a 3.2 mm front glass cover, top and bottom 0.46 mm EVA film, and a 0.5 mm back sheet.

DOI: 10.1021/acsphotonics.7b00089
ACS Photonics 2017, 4, 774−782

encapsulation layers were chosen according to commercial solar panel standards.

The solar absorption and thermal emissivity spectra of the bare cells and the encapsulated cell are experimentally characterized and shown in Figure 2a and b, respectively. In the solar wavelength region, both of the bare cells show strong light absorption from 0.3 to 1.1 μm, where the photon energy is above the silicon band gap, as expected. In the wavelength range between 1.1 and 1.8 μm, both of the bare cells show significant absorption, even though photons at these wavelength ranges have energy below the silicon band gap. Such a strong sub-band-gap absorption is in contrast with measured data on a bare silicon wafer with planar antireflection coating and metallic back reflector,[17] most likely due to the presence of metal contacts and heavily doped regions in the cells. The sub-band-gap absorption may be further enhanced by the light-trapping effects induced by surface textures.[36] From the measured absorption spectra, under AM1.5 illumination, the sub-band gap absorption of cells I and II is calculated to be 85 and 150 W/m^2, respectively. Such sub-band-gap absorption represents a parasitic heat source that does not contribute to current generation.

Compared to the bare cell, the encapsulated cell shows an even stronger absorption in the sub-band-gap as well as UV wavelength range. Our fabricated encapsulated cell has a sub-band-gap absorption of 110 W/m^2 for the AM1.5 illumination, which is significantly higher than that of the bare cell I (Figure 2a). This is due to the fact that EVA strongly absorbs UV light with a wavelength shorter than 0.375 μm and slightly absorbs in the near-infrared regime.[38] Such absorption can lead to excess heat generation while also degrading the EVA, reducing the lifetime of the solar panels. Therefore, for cooling purposes, and also to enhance the lifetime of encapsulated cell, it is beneficial to suppress the sub-band-gap and UV absorption of the solar panel while preserving or even enhancing the absorption of the solar cell in the wavelength range of 0.375−1.1 μm.

In the infrared wavelength range between 2 and 25 μm, the emissivity spectra of the bare solar cells and encapsulated cell are shown in Figure 2b. Both the bare and the encapsulated cells show strong absorption and hence strong thermal emission in the thermal wavelength range. Such an absorption spectrum again differs significantly as compared with a planar silicon wafer measured in ref 17. For the bare cells, although silicon is a weak absorbing material in this regime, the presence of a highly doped silicon region, metal contacts, and antireflection layers, usually made with SiN or SiO_2, all of which have nonzero absorption in the thermal wavelength range, together with the light-trapping effect, result in higher absorptivity/emissivity of the solar cells in the thermal wavelength range as compared to the planar silicon wafers measured in ref 17. For the encapsulated cell, its thermal emissivity is even higher in most of the wavelength range between 2 and 25 μm and is mainly determined by the 3.2 mm thick front glass layer, which contains 70−80% silica.[39] As shown in Figure 2b, the measured emissivity spectrum of the encapsulated cell is very similar to the measured or calculated emissivity spectra of fused silica.[16,17]

To summarize this section, a commercial bare solar cell has strong sub-band-gap absorption in the solar wavelength range, as well as substantial thermal emission in the wavelength range of 2−25 μm. Encapsulation of solar cells, as is required in photovoltaic modules, further enhances the sub-band-gap solar absorption and the thermal emission and in addition enhances the solar absorption in the UV wavelength range.

From the perspective of thermal management, the presence of strong solar absorption in the sub-band-gap and UV wavelength range is detrimental since this absorption represents a parasitic heat source. The presence of high emissivity in the thermal wavelength range is beneficial. It is important to note, however, that the thermal emissivity spectra of commercial solar cells, even in the best-case scenario with the encapsulation layer, are suboptimal. As was pointed out in refs 16 and 17, the emissivity exhibits a large dip near 9 μm due to the bulk phonon−polariton excitation of silica. This dip coincides with the transparency window of the atmosphere. References 16 and 17 have sought to maximize the thermal emissivity of the silica layer by surface patterning. Such an approach is difficult to implement as a retrofit on existing panels and also does not address the parasitic solar absorption issues that exist in commercial solar cells.

OUR APPROACH

On the basis of the experimental characterization of commercial solar cells as presented in the previous section, we now develop a comprehensive photonic approach for the thermal management of solar cells. We propose to add a multilayer dielectric stack on top of an existing encapsulated solar panel. This approach can be used as a retrofit: it does not require any modification of existing structures or materials in standard encapsulated cells.

For optimal thermal management purposes, the added photonic structure needs to satisfy the following design criteria as shown in Figure 3a. First, in the solar wavelength range, the photonic structure needs to have a tailored transmission/reflection characteristic. In the wavelength ranges of 0.3−0.375 μm and 1.1−4 μm, the photonic structure needs to have maximized reflection to reduce the parasitic heat generation. In the wavelength range of 0.375−1.1 μm, where photons can be converted into photocurrent, the photonic structure needs to have minimum reflection to reduce the reflection loss. Second, to maximize the radiative cooling performance of the solar cell, the photonic structure needs to have maximized emissivity in the thermal wavelength range beyond 4 μm. In order to satisfy these criteria, we note the following considerations: First, the constituent materials all need to be transparent over the solar wavelength, yet some need to be lossy over the thermal wavelength. Second, to create large solar reflection over the sub-band-gap wavelength range, materials with large index contrast need to be used. Third, over the thermal wavelength range, many lossy dielectrics such as silica have a strong phonon−-polariton response, which results in a negative permittivity that leads to large reflectivity and hence low emissivity. Therefore, one needs to combine dielectrics with both positive and negative permittivity to avoid the large reflection. Finally, all the materials should be commonly used dielectrics for cost consideration and should be amenable to large-area fabrication. Taking into account all these considerations, for our multilayer design we choose to use the dielectric materials of silica, alumina, titania, and silicon nitride.[40−42]

We perform an extensive numerical optimization procedure to achieve the photonic cooler design schematically shown in Figure 3b. The photonic cooler is on a glass substrate representing the top layer of an encapsulated solar cell and consists of alternating layers of Al_2O_3/SiN/TiO_2/SiN with

DOI: 10.1021/acsphotonics.7b00089
ACS Photonics 2017, 4, 774−782

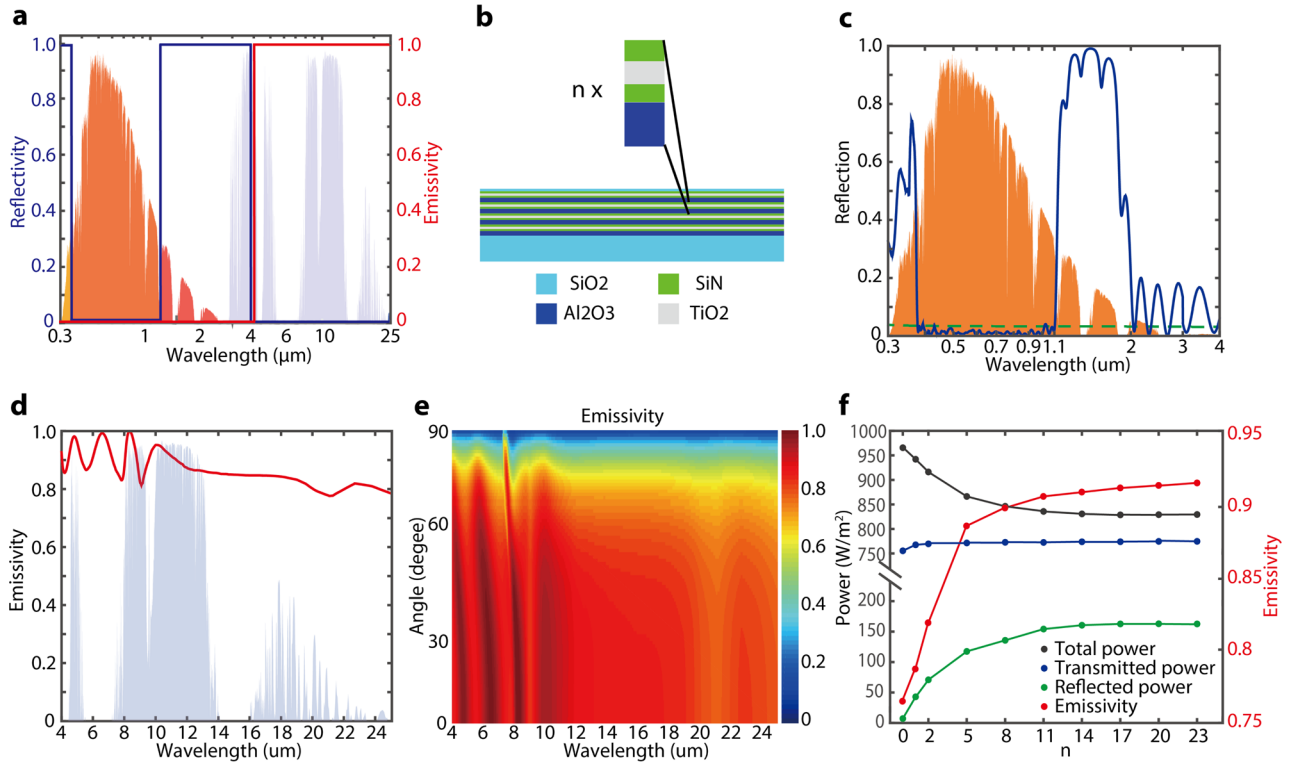

Figure 3. (a) Ideal reflection (blue) and emissivity (red) spectra of a photonic cooler, with the normalized AM1.5 solar spectrum and a realistic atmosphere transmittance model for winter in California from ref 37 plotted as the orange and the light blue shaded areas. The wavelength is plotted with a logarithmic scale for clarity. (b) Schematic of a photonic cooler made of a multilayer dielectric stack, with n sublayers. Each sublayer is made of Al_2O_3/SiN/TiO_2/SiN and a single SiO_2 layer on top. The photonic cooler is on a glass substrate. The structure thickness is aperiodic for optimized performance. (c) Reflection spectrum of the photonic cooler (blue) with n = 11 sublayers. The reflection spectrum of a glass substrate without a photonic cooler (dashed green) is plotted for reference. The wavelength is plotted with a logarithmic scale for clarity. (d) Emissivity spectra of the photonic cooler over the infrared wavelength, with a realistic atmosphere transmittance model for winter in California from ref 37 plotted as the shaded area. (e) Angle-dependent emissivity spectra of the photonic cooler over the infrared wavelength. (f) Total solar power (black dots), transmitted solar power in the wavelength range of 0.375−1.1 μm (blue dots), reflected parasitic solar power in the wavelength ranges of 0.3−0.375 μm and 1.1−4 μm (green dots), and average emissivity ε (red dots) between 8 and 13 μm, as a function of n. Data points are connected by lines for visualization.

aperiodic arrangement of thickness, with a single top layer of SiO_2 for antireflection purpose. The use of an aperiodic structure, as opposed to a periodic structure, serves to minimize the reflection oscillation in the wavelength range of 0.375 to 1.1 μm. The layer thickness of the design is presented in Supporting Information Table S1. The calculated solar reflectivity and thermal emissivity spectra of this structure are shown in Figure 3c and d, respectively. Over the solar spectrum, the structure exhibits strong reflection in the sub-band-gap and UV wavelength range. In the wavelength range of 0.375 to 1.1 μm, this cooler also serves as a broadband antireflection coating and enhances the solar transmission, as compared to the case without coating (dashed green curve in Figure 3c). In this wavelength range, the transmitted power through this photonic cooler is calculated as 772.6 W/m^2, which is more than the case without the photonic cooler, 755.5 W/m^2. In the wavelength range between 1.3 and 1.8 μm, the cooler structure shows a reflectivity that is near unity, which is important in suppressing the parasitic absorption and heat generation from part of the solar spectrum that is below the silicon band gap. Over the thermal wavelength, this cooler also shows a broadband high emissivity (Figure 3d). In particular, over the 8−13 μm atmosphere's transparency window, this cooler shows remarkably high emissivity, as opposed to silica, and this high emissivity persists to large angles (Figure 3e), a useful feature to maximize the radiative cooling power and reminiscent of the behavior of hyperbolic metamaterials.[43] The performance of this cooler can be even further enhanced by adding more layers (Figure 3f) or using other materials.[19] It should also be noted that, here, the photonic cooler is optimized for photovoltaic modules with solar irradiance from normal or with small incident angles. However, it can also be designed to work for photovoltaic modules with large incident angle ranges without having reflection loss in the useful solar spectrum from 0.375 to 1.1 μm (Supporting Information Figure S1).

We then perform a thermal analysis to calculate the cooling effect from this photonic cooler when it is integrated on top of a real solar panel (see the Methods section). Here, since the in-plane temperature variation over the solar cell is sufficiently small, we can use a one-dimensional thermal model for simplicity. It should also be noted that, in the wavelength range of 0.375 to 1.1 μm, the refractive index of the EVA layer is closely matched to the glass and the refection from the solar cell surface is sufficiently small due to the surface texturing. As a result, the solar reflection characteristics of this photonic cooler can be largely preserved when it is integrated on top of the solar panel. Therefore, we can calculate the absorbed solar power in the solar cell based on the solar reflection characteristics of this photonic cooler and experimentally measured solar cell

DOI: 10.1021/acsphotonics.7b00089
ACS Photonics 2017, 4, 774−782

absorptivity and use it as the heat input in the thermal simulation (see the Methods section). We then set up a finite-difference-based thermal simulator on a solar panel model (Figure 4a), with which we can simulate the temperature distribution across the five layers in the solar panel along the vertical direction (Figure 4b) by solving the steady-state heat diffusion equation. In particular, we choose the nonradiative heat transfer coefficients as h_1 = 10 W/m^2/K and h_2 = 5 W/m^2/K and the ambient temperature as 298 K to mimic a typical outdoor condition.[44] As shown in Figure 4b, the temperature across a solar panel can be significantly reduced by applying a photonic cooler on the top surface. We also calculate the cell operating temperature by spatially averaging the temperature inside the solar cell region. As a result, the cell operating temperature can readily be lowered by 5.7 K with the current photonic cooler design and by 8.6 K with an ideal photonic cooler (Figure 3a). For a 22% efficiency silicon solar cell with a temperature coefficient of 0.45%,[6] this 5.7 K temperature reduction can provide an absolute efficiency improvement of 0.56%, without the need of modifying the current solar panel configuration. Together with the solar transmission enhancement in the wavelength range of 0.375 to 1.1 μm, the overall absolute efficiency improvement is estimated to be around 1%. In the solar cell industry, an improvement of the absolute efficiency by one percentage point is very significant. For example, the record module efficiency for commercial crystalline silicon panels increased from about 22.7% in 2006[45] to about 23.8% in 2016,[46] or about one percentage point over a decade of intensive investments. Our work in highlighting a new theoretical pathway for one percentage point improvement in module efficiency therefore represents a significant advancement. It should also be noted that, here, the calculation is based on the encapsulated cell made of cell I, which has a much smaller sub-band-gap absorption (85 W/m^2) compared to cell II (150 W/m^2). For solar panels made of cell II, a much more significant cooling effect with a temperature reduction of 7.7 K and hence an even larger efficiency gain can be achieved (Supporting Information Figure S2).

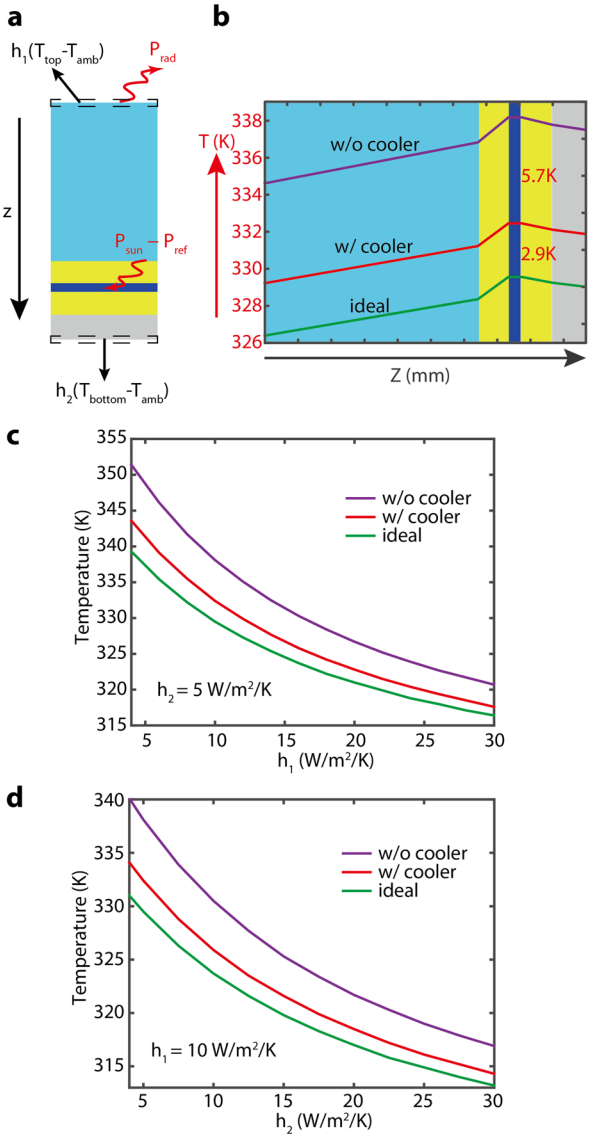

Figure 4. (a) Schematic of thermal simulation for a solar panel. h_1 and h_2 are the nonradiative heat transfer coefficients at the top and bottom surfaces, respectively. (b) Under AM1.5 illumination, simulated temperature distribution across a solar panel without a photonic cooler (purple), with a photonic cooler (red), and in the ideal situation (green), respectively. The nonradiative heat transfer coefficients in this calculation are h_1 = 10 W/m^2/K and h_2 = 5 W/m^2/K. The top and bottom ambient temperatures are both 298 K. (c) Under AM1.5 illumination, operating temperature of the solar panel, without a photonic cooler (purple), with a photonic cooler (red), and in the ideal situation (green), as a function of h_1, with a fixed h_2 = 5 W/m^2/K. (d) Under AM1.5 illumination, operating temperature of the solar panel, without a photonic cooler (purple), with a photonic cooler (red), and in the ideal situation (green), as a function of h_2, with a fixed h_1 = 10 W/m^2/K.

To further understand the cooling effects under various heat transfer conditions, we also calculate the cell operating temperature as a function of nonradiative heat transfer coefficient at the top (Figure 4c) and bottom surface (Figure 4d). This photonic cooling can still have a significant impact even in the presence of significant nonradiative cooling. For instance, when the back side of solar panel has a strong nonradiative heat transfer coefficient h_2 = 30 W/m^2/K, which corresponds to a wind speed of 9 m/s (ref 25), our photonic cooler can still achieve a temperature reduction of 3.1 K (Figure 4d), indicating its potential of being used in conjunction with other nonradiative cooling techniques.

So far we have shown that our photonic cooling approach can be used for cooling of nonconcentrated, flat solar panels. Interestingly, this technique can be even more beneficial in concentrated photovoltaic systems (CPVs)[47] where the thermal management is more critical. In this case, the primary benefit of our photonic cooling approach arises from suppressing the sub-band-gap solar absorption. Here we focused on low- and medium-concentration systems (2×−100×). In this concentration range, silicon is a commonly used cell material since it leverages the huge investment already made in the silicon supply chain and reduces the development cost.[47] As schematized in Figure 5a, here we consider a concentration system with a half-incidence angle of up to 30°, corresponding to roughly an upper limit of a typical high-efficiency Fresnel-based concentrator.[48] In this off-normal incident angle range, the thermal emissivity spectra of the photonic cooler remain nearly unchanged (Figure 3e) and the solar reflectivity spectra will slightly blue shift. However, this shift can be easily compensated by modifying the photonic design (Supporting Information Table S1). As shown in Figure 5b, the redesigned photonic cooler can efficiently reduce the sub-band-gap solar

DOI: 10.1021/acsphotonics.7b00089
ACS Photonics 2017, 4, 774−782

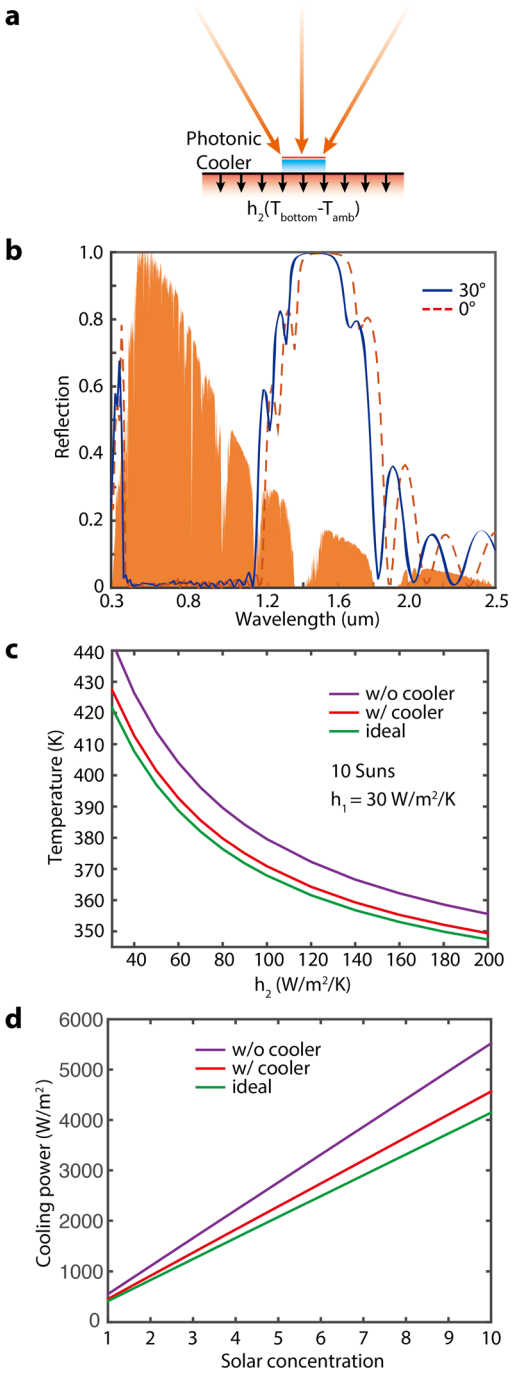

Figure 5. (a) Schematic of photonic cooling in a low-concentration photovoltaic system. (b) Reflection spectrum of the photonic cooler as a function of half-incident angle up to 30°. (c) Under 10 Suns intensity, operating temperature of the solar panel, without a photonic cooler (purple), with a photonic cooler (red), and in the ideal situation (green), as a function of h_2, with a fixed h_1 = 30 W/m^2/K. (d) To maintain the solar cell at ambient temperature, the required cooling power for a solar panel without a photonic cooler (purple), with a photonic cooler (red), and in the ideal situation (green), as a function of solar concentration.

absorption while preserving the high transmission from 0.375 to 1.1 μm for all the incident angles up to 30°. For this cooler structure design, we then perform the thermal analysis to see its cooling ability. We consider a CPV system with 10 Suns intensity concentration and an incident angle range from 0° to 30° (Supporting Information Figure S3). In this case, we consider both strong top and bottom nonradiative heat transfer coefficients to take into account other conventional cooling mechanisms such as a backside finned heat exchanger or forced convection. We calculate the cell operating temperature as a function of bottom nonradiative heat transfer coefficient h_2, as shown in Figure 5c. Remarkably, this photonic cooler can reduce the cell temperature by 15.4 K when h_2 is 30 W/m^2/K. Even when h_2 is over 200 W/m^2/K, it can still significantly reduce the cell temperature by as much as 6.2 K, indicating its potential of being used in conjunction with other cooling techniques. For a 22% efficiency silicon solar cell with a temperature coefficient of 0.45%, the temperature reductions of 15.4 and 6.2 K can provide absolute efficiency improvements of 1.52% and 0.61%, respectively. Alternatively, in a CPV system the operating temperature needs to be maintained at a fixed value and active cooling techniques such as water cooling[10] need to be employed. This photonic cooler can be used to significantly save the required cooling power (Figure 5d), and remarkably, the cooling effect will linearly scale up with the system concentration ratio (Figure 5d) and therefore can potentially play a significant role in thermal management of a CPV system.

DISCUSSION

We have introduced a comprehensive photonic approach for cooling solar cells in a solar panel scheme by simultaneously enhancing the radiative cooling while also reducing the parasitic solar absorption. We propose a cost-effective photonic design made of a multilayer dielectric stack to fulfill this requirement. We show that this photonic cooler can retrofit into an existing solar panel and efficiently reduce the cell temperature. This technique can passively cool both nonconcentrated and concentrated photovoltaic systems and can be used in conjunction with other conventional cooling mechanisms. As a proof of principle, we have designed a multilayer structure made of Al_2O_3, SiN, TiO_2, and SiO_2. However, this photonic cooler can potentially be realized with other materials that can be even more cost-effective. For instance, many polymers are strongly absorbing in the thermal wavelength range and may naturally have good radiative cooling abilities,[19] and all-polymer multilayer films[49,50] have been employed as mirrors in CPV systems. Therefore, designing our photonic cooler with all-polymer multilayer films[49,50] may even further improve the cooling performance and be more suitable for mass production.

Although here we have focused on silicon solar cells, this photonic cooler in principle can be redesigned and applied to any solar cell and is especially beneficial for cells with larger band gap energy where the amount of sub-band-gap solar energy is more significant and hence the parasitic heating effect from the sub-band-gap energy can be significant. In addition, the cooling effect of our approach can be much more significant on solar cells in space applications, where the radiative access to the sun and the universe is the dominant heating exchange mechanism.

More generally, our strategy provides a universal approach for cooling any outdoor object where sunlight utilization is intrinsic either for functional or aesthetic purposes. For applications where the object color needs to be preserved, only the visible transparency is required and over half of the total solar power serves as a parasitic heat source. In this case, our photonic cooler can be easily redesigned to selectively transmit the visible spectrum while also radiatively cooling the

DOI: 10.1021/acsphotonics.7b00089
ACS Photonics 2017, 4, 774−782

object. Hence our approach here can potentially be very important for applications such as automobile cooling, where the need for air-conditioning can reduce fuel economy by 20%.[51] Finally, previous radiative cooling work has shown the ability to control the thermal radiation and solar absorption properties independently, for example, completely reflecting the solar spectrum, making no use of sunlight,[29] or completely transmitting the solar spectrum.[16,17] Here we show that radiative cooling can be used in conjunction with a more carefully engineered solar energy harvesting. Our approach represents a step forward in simultaneously exploiting both radiative cooling and solar energy harvesting.

METHODS

Solar Cell Encapsulation and Characterization. To perform the solar cell encapsulation, a solar cell is sandwiched between two 0.46 mm thick EVA films and then covered with a 3.2 mm thick glass on the top and a 0.5 mm thick back sheet on the bottom, as schematized in Figure 2d. Then the sample is heated to 150 °C in vacuum conditions for 10 min and naturally cooled to get the final encapsulated cell. In the wavelength range of 0.3−1.8 μm, the solar reflectance and transmittance of both bare cells and the encapsulated cell were characterized using a spectrophotometer (Agilent Cary 6000i) with an unpolarized light source and a high Lambertian reflectance standard (Labsphere SRS-99-020). A diffuse reflectance accessory (DRA 1800) with a 150-mm-diameter integrating sphere was used to collect both specular and diffuse components of reflection at an 8° angle of incidence. In the wavelength range of 2−25 μm, a Fourier transform infrared spectrometer (Thermo Scientific Nicolet 6700) accompanied by a diffuse gold integrating sphere (PIKE Technologies) was used to characterize the reflectance and transmittance of both bare and encapsulated cells. The absorptivity/emissivity spectra were obtained by subtracting the reflectance and transmittance from unity.

Thermal Calculation of Solar Cells. We perform a thermal analysis to calculate the cooling effect from this photonic cooler in a real solar panel scheme. Here, since the in-plane temperature variation over the solar cell is sufficiently small, we can use a one-dimensional thermal model for simplification. We set up a finite-difference-based thermal simulator over a five-layer solar panel model (Figure 4a), where we can simulate the temperature distribution across the solar panel in the vertical direction by solving the steady-state heat diffusion equation:

$$\frac{\mathrm{d}}{\mathrm{d}x}\left[k(z)\frac{\mathrm{d}T(z)}{\mathrm{d}z}\right] + \dot{q}(z) = 0 \tag{1}$$

where $T(z)$ is the temperature distribution across the solar panel. Here the thermal conductivity values of glass, EVA, a silicon solar cell, and Tedla are 0.98, 0.24, 148, and 0.36 W/m/K, respectively, according to ref 52. We apply the thermal boundary condition at the top surfaces of the solar panel as

$$-k(z)\frac{\mathrm{d}T(z)}{\mathrm{d}z}\bigg|_{\mathrm{top}} = P_{\mathrm{cooling}}(T_{\mathrm{top}}) + h_1(T_{\mathrm{top}} - T_{\mathrm{amb}}) \tag{2}$$

to take into account both the radiative cooling effect $P_{\mathrm{cooling}}(T_{\mathrm{top}})$ and additional nonradiative heat dissipation due to convection and conduction, as characterized by $h_1(T_{\mathrm{top}} - T_{\mathrm{amb}})$. At the lower surface, we assume a boundary condition

$$k(z)\frac{\mathrm{d}T(z)}{\mathrm{d}z}\bigg|_{\mathrm{bottom}} = h_2(T_{\mathrm{bottom}} - T_{\mathrm{amb}}) \tag{3}$$

to characterize the nonradiative heat loss of the lower surface.

On the basis of the solar absorptivity and thermal emissivity spectra of the encapsulated cell and the photonic cooler, we can first calculate the total solar absorption and radiative cooling power of the solar panels by

$$P_{\mathrm{sun}} = \int_0^\infty \mathrm{d}\lambda\, I_{\mathrm{AM1.5}}(\lambda)\, \varepsilon(\lambda, \theta_{\mathrm{sun}})\, (1 - r(\lambda, \theta_{\mathrm{sun}}))\cos\theta_{\mathrm{sun}} \tag{4}$$

where P_{sun} is the solar absorption power, $I_{\mathrm{AM1.5}}(\lambda)$ is the AM1.5 spectrum, $\varepsilon(\lambda, \theta_{\mathrm{sun}})$ is the solar absorptivity of the solar cell, $r(\lambda, \theta_{\mathrm{sun}})$ is the reflectivity spectrum of the photonic cooler, and θ_{sun} is the solar incidence angle. Here we assume the heat is uniformly generated in the solar cell, and we can obtain $\dot{q}(z)$ in eq 1. Meanwhile, the top surface radiative cooling power P_{cooling} can be calculated as

$$P_{\mathrm{cooling}}(T_{\mathrm{top}}) = P_{\mathrm{rad}}(T_{\mathrm{top}}) - P_{\mathrm{atm}}(T_{\mathrm{amb}}) \tag{5}$$

P_{rad} is the total thermal radiation power by the solar panel and can be calculated as

$$P_{\mathrm{rad}}(T_{\mathrm{top}}) = \int \mathrm{d}\Omega \cos\theta \int_0^\infty \mathrm{d}\lambda\, I_{\mathrm{BB}}(T_{\mathrm{top}}, \lambda)\, \varepsilon(\lambda, \Omega) \tag{6}$$

where $\int \mathrm{d}\Omega = \int_0^{\pi/2} \mathrm{d}\theta \sin\theta \int_0^{2\pi} \mathrm{d}\phi$ is the angular integral over the hemisphere. $I_{\mathrm{BB}}(T, \lambda) = (2hc^2/\lambda^5)/[\mathrm{e}^{hc/\lambda K_{\mathrm{B}}T} - 1]$ is the spectral radiance of a blackbody at temperature T, where h is Planck's constant, c is the velocity of light, and K_{B} is the Boltzmann constant.

P_{rad} is the absorbed thermal emission power from the atmosphere and can be calculated as

$$P_{\mathrm{atm}}(T_{\mathrm{amb}}) = \int \mathrm{d}\Omega \cos\theta \int_0^\infty \mathrm{d}\lambda\, I_{\mathrm{BB}}(T_{\mathrm{amb}}, \lambda)\, \varepsilon(\lambda, \Omega)\, \varepsilon_{\mathrm{atm}}(\lambda, \Omega) \tag{7}$$

where $\varepsilon_{\mathrm{atm}}(\lambda, \Omega) = 1 - t(\lambda)^{1/\cos\theta}$ is the angular-dependent emissivity of the atmosphere and $t(\lambda)$ is the atmosphere's transmittance in the zenith direction.

The solution of the heat equation results in a temperature distribution $T(z)$ shown in Figure 4b. The operating temperature of the solar cell (Figure 4c and d) is then defined as the spatially averaged temperature inside the solar cell region.

ASSOCIATED CONTENT

Supporting Information

The Supporting Information is available free of charge on the ACS Publications website at DOI: 10.1021/acsphotonics.7b00089.

Figures of photonic cooler design for large incident angles, photonic cooling effects on photovoltaic modules made of cell II, and concentrated photovoltaic system design with 10× concentration factor and 30° half-incident angle; table of layer thickness parameters for various photonic cooler designs (PDF)

AUTHOR INFORMATION

Corresponding Author

*E-mail (S. Fan): shanhui@stanford.edu.

DOI: 10.1021/acsphotonics.7b00089
ACS Photonics 2017, 4, 774−782

ORCID

Wei Li: 0000-0002-2227-9431

Notes

The authors declare no competing financial interest.

■ ACKNOWLEDGMENTS

This work was supported by the Department of Energy Grants No. DE-FG-07ER46426 and DE-EE0007544. The authors thank John Stayner for assistance with the solar cell encapsulation process.

■ REFERENCES

(1) Shockley, W.; Queisser, H. J. Detailed Balance Limit of Efficiency of p-n Junction Solar Cells. *J. Appl. Phys.* **1961**, *32*, 510.
(2) Davis, M. W.; Fanney, A. H.; Dougherty, B. P. Prediction of Building Integrated Photovoltaic Cell Temperatures. *J. Sol. Energy Eng.* **2001**, *123*, 200−210.
(3) Ingersoll, J. G. Simplified Calculation of Solar Cell Temperatures in Terrestrial Photovoltaic Arrays. *J. Sol. Energy Eng.* **1986**, *108*, 95−101.
(4) Jones, A. D.; Underwood, C. P. A thermal model for photovoltaic systems. *Sol. Energy* **2001**, *70*, 349−359.
(5) Dupré, O., Vaillon, R., Green, M. A. Thermal Issues in Photovoltics and Existing Solutions. In *Thermal Behavior of Photovoltaic Devices*; Springer International Publishing, 2017; pp 1−28.
(6) Skoplaki, E.; Palyvos, J. A. On the temperature dependence of photovoltaic module electrical performance: A review of efficiency/power correlations. *Sol. Energy* **2009**, *83*, 614−624.
(7) Otth, D. H.; Ross, R. G.Assessing photovoltaic module degradation and lifetime from long term environmental tests. *Proceedings of the 1983 Institute of Environmental Sciences 29th Annual Technical Meeting*; 1983; pp 121−126.
(8) Royne, A.; Dey, C. J.; Mills, D. R. Cooling of photovoltaic cells under concentrated illumination: a critical review. *Sol. Energy Mater. Sol. Cells* **2005**, *86*, 451−483.
(9) Teo, H. G.; Lee, P. S.; Hawlader, M. N. A. An active cooling system for photovoltaic modules. *Appl. Energy* **2012**, *90*, 309−315.
(10) Moharram, K. A.; Abd-Elhady, M. S.; Kandil, H. A.; El-Sherif, H. Enhancing the performance of photovoltaic panels by water cooling. *Ain Shams Eng. J.* **2013**, *4*, 869−877.
(11) Akbarzadeh, A.; Wadowski, T. Heat pipe-based cooling systems for photovoltaic cells under concentrated solar radiation. *Appl. Therm. Eng.* **1996**, *16*, 81−87.
(12) Zhang, Y.; Du, Y.; Shum, C.; Cai, B.; Le, N.; Chen, X.; Duck, B.; Fell, C.; Zhu, Y.; Gu, M. Efficiently-cooled plasmonic amorphous silicon solar cells integrated with a nano-coated heat-pipe plate. *Sci. Rep.* **2016**, *6*, 24972.
(13) Mullaney, K., Jones, G., Kitchen, C. A., Jones, D. P. Infra-red reflective coverglasses: the next generation. In *Photovoltaic Specialists Conference, 1993, Conference Record of the Twenty Third IEEE*; 1993; pp 1363−1368.
(14) Beauchamp, W., Tuttle-Hart, T. UV/IR reflecting solar cell cover. UV/IR reflecting solar cell cover. *US Pat.* 5, 449, 413, 1995.
(15) Yoon, H., Joslin, D. E., Law, D. C., Krut, D., King, R. R., Vijayakumar, P., Peterson, D., Hanley, J., Karam, N. H. Application of infrared reflecting (IRR) coverglass on multijunction III-V solar cells. In *2006 IEEE 4th World Conference on Photovoltaic Energy Conference*; 2006; pp 1861−1864.
(16) Zhu, L.; Raman, A.; Wang, K. X.; Anoma, M. A.; Fan, S. Radiative cooling of solar cells. *Optica* **2014**, *1*, 32.
(17) Zhu, L.; Raman, A. P.; Fan, S. Radiative cooling of solar absorbers using a visibly transparent photonic crystal thermal blackbody. *Proc. Natl. Acad. Sci. U. S. A.* **2015**, *112*, 12282−12287.
(18) Safi, T. S.; Munday, J. N. Improving photovoltaic performance through radiative cooling in both terrestrial and extraterrestrial environments. *Opt. Express* **2015**, *23*, A1120.
(19) Wu, S.-H.; Povinelli, M. L. Solar heating of GaAs nanowire solar cells. *Opt. Express* **2015**, *23*, A1363.
(20) Bermel, P.; Boriskina, S. V.; Yu, Z.; Joulain, K. Control of radiative processes for energy conversion and harvesting. *Opt. Express* **2015**, *23*, A1533.
(21) Catalanotti, S.; Cuomo, V.; Prio, G.; Ruggi, D.; Silvestrini, V.; Troise, G. The radiative cooling of selective surfaces. *Sol. Energy* **1975**, *17*, 83−89.
(22) Harrison, A. W., Walton, M. R. *Radiative cooling of TiO_2 white paint. Solar Energy*; Pergamon, 1978; Vol. *20*.
(23) Granqvist, C. G.; Hjortsberg, A. Radiative cooling to low temperatures: General considerations and application to selectively emitting SiO films. *J. Appl. Phys.* **1981**, *52*, 4205−4220.
(24) Nilsson, T. M. J.; Niklasson, G. A.; Granqvist, C. G. A solar reflecting material for radiative cooling applications: ZnS pigmented polyethylene. *Sol. Energy Mater. Sol. Cells* **1992**, *28*, 175−193.
(25) Nilsson, T. M. J.; Niklasson, G. A. Radiative cooling during the day: simulations and experiments on pigmented polyethylene cover foils. *Sol. Energy Mater. Sol. Cells* **1995**, *37*, 93−118.
(26) Gentle, A. R.; Aguilar, J. L. C.; Smith, G. B. Optimized cool roofs: Integrating albedo and thermal emittance with R-value. *Sol. Energy Mater. Sol. Cells* **2011**, *95*, 3207−3215.
(27) Zhu, L.; Raman, A.; Fan, S. Color-preserving daytime radiative cooling. *Appl. Phys. Lett.* **2013**, *103*, 223902.
(28) Rephaeli, E.; Raman, A.; Fan, S. Ultrabroadband Photonic Structures To Achieve High-Performance Daytime Radiative Cooling. *Nano Lett.* **2013**, *13*, 1457−1461.
(29) Raman, A. P.; Anoma, M. A.; Zhu, L.; Rephaeli, E.; Fan, S. Passive radiative cooling below ambient air temperature under direct sunlight. *Nature* **2014**, *515*, 540−544.
(30) Tong, J. K.; Huang, X.; Boriskina, S. V.; Loomis, J.; Xu, Y.; Chen, G. Infrared-Transparent Visible-Opaque Fabrics for Wearable Personal Thermal Management. *ACS Photonics* **2015**, *2*, 769−778.
(31) Shi, N. N.; Tsai, C.-C.; Camino, F.; Bernard, G. D.; Yu, N.; Wehner, R. Keeping cool: Enhanced optical reflection and radiative heat dissipation in Saharan silver ants. *Science* **2015**, *349*, 298−301.
(32) Chen, Z.; Zhu, L.; Raman, A.; Fan, S. Radiative cooling to deep sub-freezing temperatures through a 24-h day−night cycle. *Nat. Commun.* **2016**, *7*, 13729.
(33) Saga, T. Advances in crystalline silicon solar cell technology for industrial mass production. *NPG Asia Mater.* **2010**, *2*, 96−102.
(34) Smith, D., Cousins, P., Masad, A., Westerberg, S., Defensor, M., Ilaw, R., Dennis, T., Daquin, R., Bergstrom, N., Leygo, A., Zhu, X., Meyers, B., Bounre, B., Shields, M., Rose, D. SunPower's Maxeon Gen III solar cell: high efficiency and energy yield. *Proceedings of IEEE 39th Photovoltaic Specialists Conference (PVSC) 16−21 June 2013, Tampa, Florida*; 2013; pp 0908−13.
(35) Neuhaus, D. H.; Münzer, A. Industrial silicon wafer solar cells. *Adv. OptoElectron.* **2007**, *2007*, 1−15.
(36) Campbell, P.; Green, M. A. Light trapping properties of pyramidally textured surfaces. *J. Appl. Phys.* **1987**, *62*, 243.
(37) Berk, A.; Anderson, G. P.; Acharya, P. K.; Bernstein, L. S.; Muratov, L.; Lee, J.; Fox, M.; Adler-Golden, S. M.; Chetwynd, J. H., Jr.; Hoke, M. L.; Lockwood, R. B.; Gardner, J. A.; Cooley, T. W.; Borel, C. C.; Lewis, P. E.; Shettle, E. P. MODTRAN5: 2006 update. *Proc. SPIE* **2006**, *6233*, 62331F−62331F-8.
(38) Miller, D. C. Analysis of transmitted optical spectrum enabling accelerated testing of multijunction concentrating photovoltaic designs. *Opt. Eng.* **2011**, *50*, 13003.
(39) Kurkjian, C. R.; Prindle, W. R. Perspectives on the History of Glass Composition. *J. Am. Ceram. Soc.* **1998**, *81*, 795−813.
(40) Palik, E. D., Ghosh, G. *Handbook of Optical Constants of Solids*; Academic Press, 1998.
(41) Kischkat, J.; Peters, S.; Gruska, B.; Semtsiv, M.; Chashnikova, M.; Klinkmüller, M.; Fedosenko, O.; Machulik, S.; Aleksandrova, A.; Monastyrskyi, G.; Flores, Y.; Masselink, W. T. Mid-infrared optical properties of thin films of aluminum oxide, titanium dioxide, silicon dioxide, aluminum nitride, and silicon nitride. *Appl. Opt.* **2012**, *51*, 6789−6798.

DOI: 10.1021/acsphotonics.7b00089
ACS Photonics 2017, 4, 774−782

(42) Devore, J. R. Refractive Indices of Rutile and Sphalerite. *J. Opt. Soc. Am.* **1951**, *41*, 416.
(43) Jacob, Z.; Kim, J.; Naik, G. V.; Boltasseva, A.; Narimanov, E. E.; Shalaev, V. M. Engineering photonic density of states using metamaterials. *Appl. Phys. B: Lasers Opt.* **2010**, *100*, 215−218.
(44) Armstrong, S.; Hurley, W. G. A thermal model for photovoltaic panels under varying atmospheric conditions. *Appl. Therm. Eng.* **2010**, *30*, 1488−1495.
(45) Green, M. A.; Emery, K.; King, D. L.; Hisikawa, Y.; Warta, W. Solar cell efficiency tables (version 27). *Prog. Photovoltaics* **2006**, *14*, 45−51.
(46) Green, M. A.; Emery, K.; Hishikawa, Y.; Warta, W.; Dunlop, E. D. Solar cell efficiency tables (version 48). *Prog. Photovoltaics* **2016**, *24*, 905−913.
(47) Kurtz, S. Opportunities and Challenges for Development of a Mature Concentrating Photovoltaic Power Industry Opportunities and Challenges for Development of a Mature Concentrating Photovoltaic Power Industry. *Technol. Rep.* NREL/TP-52, **2012**, 43208 10.2172/935595.
(48) Benítez, P.; Minano, J. C.; Zamora, P.; Mohedano, R.; Cvetkovic, A.; Buljan, M.; Chaves, J.; Hernandez, M. High performance Fresnel-based photovoltaic concentrator. *Opt. Express* **2010**, *18*, A25.
(49) Gilbert, L. R., Jonza, J. M., Ouderkirk, A. J., Stover, C. A., Weber, M. F., Merrill, W. W. Multilayer Polymer Film With Additional Coatings or Layers. *US Pat.* 6,368,699, 2002.
(50) Weber, M. F.; Stover, C. A.; Gilbert, L. R.; Nevitt, T. J.; Ouderkirk, A. J. Giant Birefringent Optics in Multilayer Polymer Mirrors. *Science* **2000**, *287*, 2451−2456.
(51) Farrington, R., Rugh, J. Impact of Vehicle Air-Conditioning on Fuel Economy, Tailpipe Emissions, and Electric Vehicle Range. *NREL/CP-540-28960*, 2000: http://www.nrel.gov/docs/fy00osti/28960.pdf.
(52) Lee, B.; Liu, J. Z.; Sun, B.; Shen, C. Y.; Dai, G. C. Thermally conductive and electrically insulating EVA composite encapsulant for solar photovoltaic (PV) cell. *eXPRESS Polym. Lett.* **2008**, *2*, 357−363.

DOI: 10.1021/acsphotonics.7b00089
ACS Photonics 2017, 4, 774−782